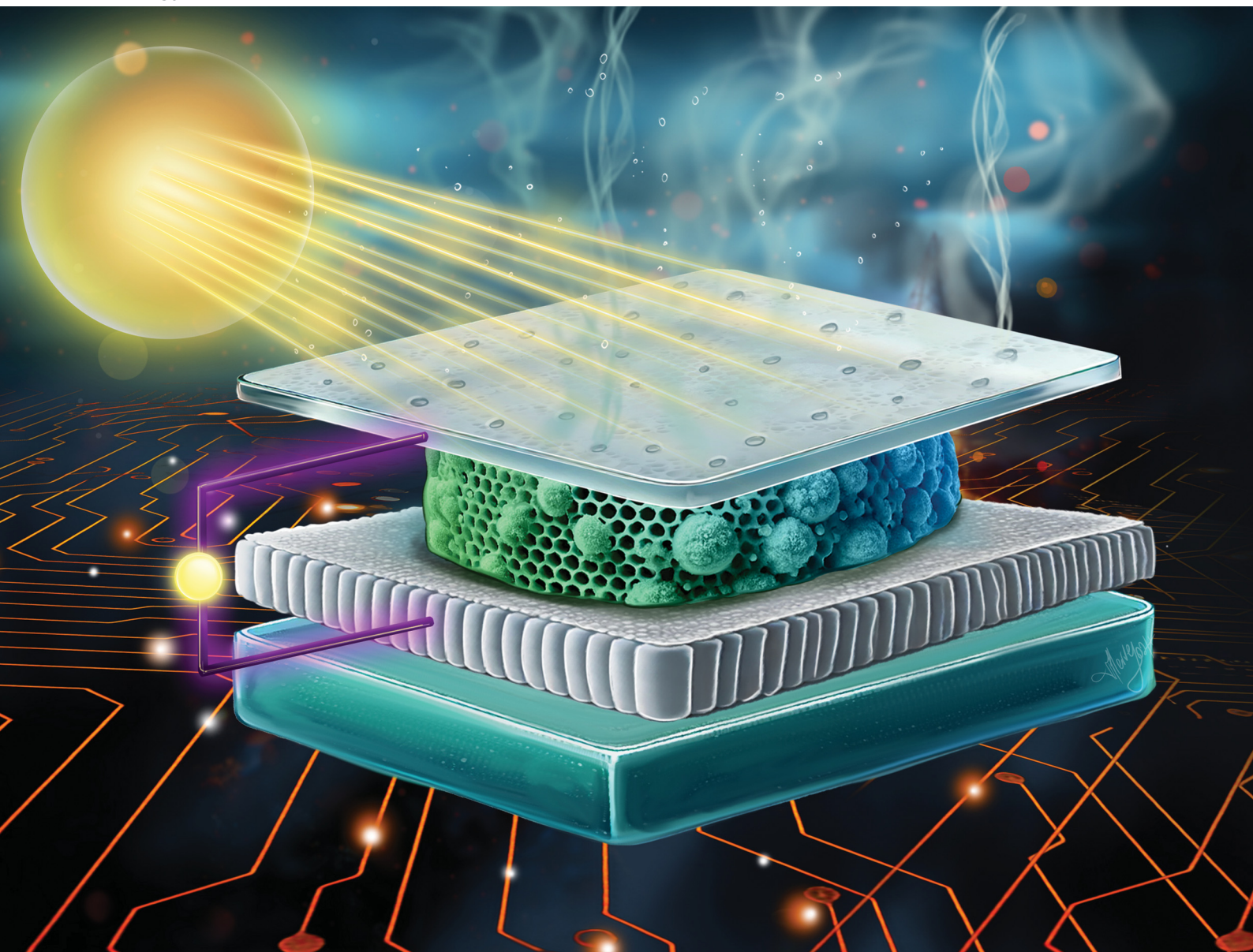


# Energy Advances

Volume 3  
Number 10  
October 2024  
Pages 2419-2660

[rsc.li/energy-advances](https://rsc.li/energy-advances)







ISSN 2753-1457

**PAPER**

Ghazaleh Gharib, Ali Koşar *et al.*  
Electricity generation using a microbial 3D bio-anode  
embedded bio-photovoltaic cell in a microfluidic chamber

Cite this: *Energy Adv.*, 2024,  
3, 2439

# Electricity generation using a microbial 3D bio-anode embedded bio-photovoltaic cell in a microfluidic chamber†

Zülal Munganlı,  ‡<sup>ab</sup> İsmail Bütün,  ‡<sup>ab</sup> Ghazaleh Gharib  \*<sup>abcd</sup> and  
Ali Koşar  \*<sup>abce</sup>

New-generation sustainable energy systems serve as major tools to mitigate the greenhouse gas emissions and effects of climate change. Biophotovoltaics (BPVs) presents an eco-friendly approach by employing solar energy to ensure self-sustainable bioelectricity. In contrast to other microbial fuel cells (MFCs), carbon feedstock is not essential for generating electricity with BPVs. However, the low power outputs ( $\mu\text{W cm}^{-2}$ ) obtained from the current systems limit their practical applications. In this study, a new generation polydimethylsiloxane (PDMS) based BPV cell unit was developed with a 3D hydrogel scaffold-based bio-anode to enable microbial biofilm formation for substantial electron capture and extracellular electron transfer. Moreover, the fabricated device was supported using an air-cathode electrode to elevate the gas exchange, thereby enabling optimum photosynthesis. *Synechocystis* sp. PCC 6803 seeded the 3D bio-anode embedded BPV cell, whose electrical characteristics were analyzed under the illumination of white light as day/night cycles with continuous feeding by the microchannel. For the first five days, the results indicated that the maximum power densities were  $0.0534 \text{ W m}^{-2}$  for dark hours and  $0.03911 \text{ W m}^{-2}$  for light hours without causing any effect on the cellular morphology of the cyanobacteria. As a result, the developed hydrogel scaffold-based bio-anode embedded BPV cell led to higher power densities *via* enabling a simple, self-sustainable, biocompatible, and eco-friendly energy harvesting platform with a possible capability in the applications of power lab-on-a-chip (LOC), point-of-care (POC), and small-scale portable electronic devices.

Received 2nd May 2024,  
Accepted 2nd September 2024

DOI: 10.1039/d4ya00278d

rsc.li/energy-advances

## 1. Introduction

The quick escalation in global energy consumption relying on fossil fuels leads to the emission of greenhouse gases (GHGs), which triggers climate change.<sup>1</sup> The development of clean and renewable energy production systems substituting fossil fuel-based energy systems is crucial for overcoming the global issue of CO<sub>2</sub> emissions and energy source deficiency.<sup>2</sup> Nowadays, microorganisms including bacteria, fungi, and

algae have a key role in sustainable bioelectricity and biofuel generation.<sup>3</sup> Biodiesel, bioethanol, bio-butanol, and bio-hydrogen could be produced as biofuels whereas microbial fuel cells (MFCs) and bio-photovoltaics (BPVs) could be involved in bioelectricity generation towards green energy *via* biomass and the metabolism of microorganisms.<sup>4–7</sup> The type of microorganism is critical to obtain higher power densities in MFCs.<sup>8</sup> Furthermore, the diversity of microorganism sources such as wastewater, freshwater, and soil makes MFCs advantageous in the generation of efficient bioenergy while having great potential in the regulation of waste management.

BPVs, also known as bio-solar cells or biological photovoltaics, were invented to generate bioenergy.<sup>9</sup> They offer an environmentally friendly approach for harnessing solar energy to convert it into electricity. Cyanobacteria, which are the best choice for the BPVs' main energy generator, are commonly considered the preferred source in this approach due to their possession of chlorophyll, which allows them to harvest solar energy for efficient electricity generation.<sup>10–12</sup> The mechanism regarding BPVs involves splitting the water molecule by utilizing the incoming light which produces electrons and protons and is

<sup>a</sup> Faculty of Engineering and Natural Sciences, Sabancı University, Turkey.

E-mail: kosara@sabanciuniv.edu, ghazalehgharib@sabanciuniv.edu

<sup>b</sup> Sabancı University Nanotechnology Research and Application Centre (SUNUM), Istanbul, Turkey<sup>c</sup> Center of Excellence for Functional Surfaces and Interfaces for Nano-Diagnostics (EFSUN), Sabancı University, Istanbul, Turkey<sup>d</sup> Faculty of Science, Department of Biology, Nordcee, University of Southern Denmark, Odense, Denmark<sup>e</sup> Turkish Academy of Sciences (TÜBA), Çankaya, 06700, Ankara, Turkey† Electronic supplementary information (ESI) available. See DOI: <https://doi.org/10.1039/d4ya00278d>

‡ Co-first authorship.



eventually collected using a bio-electrochemical system.<sup>13</sup> The operation of BPVs does not require any carbon feedstock. Only water and light are essential for generating electricity in contrast to microbial fuel cells (MFCs).<sup>14,15</sup> However, the anodic layer of bio-solar cells is a crucial parameter in capturing photons and affects the electricity generation capacity according to the type of material used as an anode layer.<sup>16</sup> The low power outputs ( $\mu\text{W cm}^{-2}$ ), a critical limitation of BPVs, suggest the implementation and combination of novel technologies.<sup>17</sup> Numerous studies have been performed to modify the electrode layer of BPVs and to boost the electrochemical interaction between electrons and living cells.<sup>12,18–21</sup>

Microfluidics involves fluid manipulation in small diameter channels<sup>22</sup> and paves the way for applications such as drug screening,<sup>23,24</sup> environmental monitoring,<sup>25</sup> and biomedical applications.<sup>26,27</sup> Furthermore, microfluidics has been also employed in microalgae studies regarding cultivation and bio-fuel production.<sup>27–29</sup> In microalgae cultivation, microfluidics offers time-efficient and cost-effective techniques with efficient cell/reagent controlling abilities and precise and high-throughput assays in an automated platform compared to the conventionally used bulky, labor-intensive cell culturing techniques.<sup>30</sup> Besides, microfluidic systems could overcome low power output and sustainability problems while the miniaturization of BPVs could result in a reduction in the internal resistance and in advancing mass transport<sup>10</sup> and could cause a significant enhancement in harvested energy. In comparison to larger-scale ones, small-unit bio-solar cells have the potential to have greater power density, and the efficiency of the obtained power can be increased by combining small-scale units.<sup>16</sup> Culture conditions such as nutrient supply, light diffusion, pH, and fluidic conditions could be easily monitored and mediated by microfluidic platforms to achieve optimum microalgal cell growth.<sup>31,32</sup>

Cyanobacteria are unique prokaryotes that are able to capture sunlight as a source of energy to metabolize water as an electron donor and air as a carbon resource.<sup>33</sup> Their significant role in biofuel production of harnessing light energy and converting  $\text{CO}_2$  into various products stems from their ability to utilize photosynthesis for energy generation.<sup>34</sup> For a long while, they have been preferred in wastewater treatment due to their advantageous features, including the absence of the need for organic carbon sources, the ability to reduce sludge formation, the improvement in reducing  $\text{CO}_2$  emissions associated with wastewater treatment facilities, and cost-effectiveness.<sup>35</sup> In current studies, cyanobacteria have been exploited to produce proteins, carotenoids, lipids, biofuels, and bioelectricity.<sup>36–40</sup> However, culturing conditions of cyanobacteria are critical for their growth and consequently, biomass production, which will be utilized for biofuel generation and production of electricity. Important parameters such as pH, nutrient ability and temperature affecting the growth should be perfectly arranged to obtain a healthy growth of cyanobacteria and efficient biomass production and  $\text{CO}_2$  capturing.<sup>41</sup>

Several cultivation strategies have been developed to improve the growth of cyanobacteria for distinctive purposes

such as the generation of protein-based techno-functional food ingredients,<sup>42</sup> the biofertilization of plants,<sup>43</sup> and the development of photobioreactor cultivation strategies.<sup>44</sup> Traditional BPV systems are utilized in a liquid environment of photosynthetic bacteria or algae which limits the interaction between the anode and microorganisms while handling a large volume and high mass of the culture.<sup>21</sup> The essential issue in the design of BPVs lies in the preparation of a solid anode compartment using a biocompatible and conductive material, eligible for the growth of microorganisms during electron transfer. In this regard, the hydrogel structure, which allows for the transmission of electrons and protons through the cathode compartment, is a common biomaterial promoting the rapid growth of the cyanobacterial culture.

Hydrogels are polymeric chains having three-dimensional (3D) structures that absorb and store a large amount of water with their hydrophilic functional groups.<sup>45</sup> Various natural, synthetic, and hybrid materials can be utilized to produce hydrogels including hyaluronic acid and cellulose as natural hydrogel, polyethylene glycol (PEG) and polyethylene oxide (PEO) as synthetic hydrogel, collagen acrylate and alginate-acrylate as hybrid hydrogels.<sup>46</sup> Alfaro-Sayes *et al.* indicated that sodium-alginate hydrogel immobilization provided the growth of cyanobacteria.<sup>47</sup> However, the application of alginate is limited due to its low mechanical strength.<sup>48</sup> Cellulose can be derived from various sources, such as bacteria, algae, plant cell walls, and tunicates.<sup>49</sup> It can appear in different forms, including nanofibrils or microfibrils, fibers, and nanocrystals or microcrystals, each differing in shape, size, and physical characteristics.<sup>49</sup> Cellulose nanofibers (CNFs), a particular structure of cellulose, stand out due to their promising properties such as exceptional mechanical strength, large surface area, and excellent oxygen barrier capabilities. Due to their transparent, biodegradable, renewable, biocompatible, and stable conductivity, cellulose-based hydrogels have attracted significant attention. The ionic conductivity of cellulose-based hydrogels and their utilization as a scaffold material opens a new avenue for applications in energy and sensing.<sup>50</sup> Furthermore, several studies reported that cellulose could be employed as a fuel to be degraded by microorganisms for current production in MFC applications (Fig. 1).<sup>51–53</sup>

In the present study, we developed a new generation polydimethylsiloxane (PDMS) based microfluidic chamber integrated with a BPV cell which is a pioneering attempt to establish a 3D biofilm formation by hydrogel scaffold-based BPV. It was aimed to achieve four essential objectives to reach higher power outputs for long-term energy generation: (1) presenting a simple preparation of 3D solid bio-anode structure, (2) developing a biocompatible 3D hydrogel-based scaffold that enables photosynthesis of the cyanobacteria, (3) having a 3D cyanobacterial biofilm formation to achieve an infinite source of energy, and (4) ensuring microfluidic feeding of the cyanobacteria for self-sustainable BPV cells. In one of the previous studies, the maximum power density was recorded as  $43.8 \mu\text{W cm}^{-2}$ , which was not sufficient to power electronic devices.<sup>18</sup> For this purpose, a circular-shaped BPV cell mechanism was developed thanks to the fabrication of a 3D hydrogel-based solid bio-anode compartment and air cathode inside a





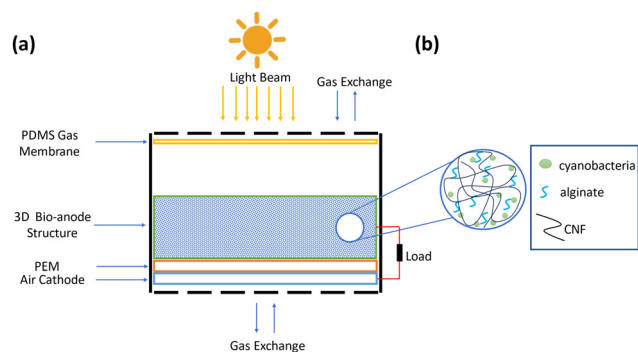


**Fig. 1** Schematic of a 3D hydrogel-based bio-anode embedded BPV cell unit for energy harvesting. (a) Schematic of 3D hydrogel-based bio-anode embedded BPV cell unit (b) components of the 3D hydrogel-based bio-anode structure.

microfluidic system. They provide supportive microenvironment, encompassing mechanical reinforcement, as well as physical and biochemical cues essential for facilitating optimal cellular proliferation and functionality.<sup>54</sup> Besides, 3D microenvironments have a critical role in biofilm formation which cyanobacteria tend to have in nature.<sup>55</sup> The 3D scaffolds present an ambient that promotes the dynamic growth of biofilms in both horizontal and vertical directions as in naturally occurring biofilms.<sup>56</sup> Therefore, a 3D environment is required to mimic the natural biofilm formation of the *Synechocystis* sp. PCC 6803 *via* promoting their proliferation. The CNF and alginate were utilized as the main scaffold materials to support the 3D biofilm formation of cyanobacteria *Synechocystis* sp. PCC 6803. The 3D biofilm formation provides an infinite source of power generation since the CNF hydrogel is transparent, which is crucial in transmitting light through cyanobacteria for activating the photosynthesis process, and is hydrophilic as well, which is vital for transmitting water in cultivation.

Therefore, CNF/alginate including scaffolds could provide the required environment to initiate the photosynthesis of cyanobacteria. CNF not only procures photosynthesis, but its conductive nature also provides the transfer of produced electrons and protons through the cathode compartment by increasing the mechanical strength of alginate hydrogel. Furthermore, increasing the air exchange between the BPV cell and the environment is essential to have the optimum condi-

tions for photosynthesis. The utilized air-cathode in the current study is composed of a mixture of carbon black (CB), activated carbon (AC), and polyvinylidene fluoride (PVDF) on a stainless steel mesh. The mesh structure helps to improve the gas exchange between the environment and the BPV unit. Furthermore, several studies have shown that air cathode integration through MFCs is a great tool to elevate the power outputs.<sup>57</sup> The utilization of air cathodes serves to increase the presence of dissolved oxygen in close proximity to the cathode while diminishing the cathodic resistance.<sup>58</sup> In addition, having a large cathode surface area on air cathodes is significant in increasing the power density.<sup>59</sup> Therefore, an air cathode, which consists of CB, AC, and PVDF was fabricated in this study. The developed electrodes were integrated into the BPV cell system. After assembling all the components, the evaluation of electrical properties was made. We focused on examining the electrical characteristics of a bacterial culture growing inside the 3D bio-anode, which was continuously fed at a flow rate of 40  $\mu\text{L min}^{-1}$  and was subjected to 16.7  $\text{W m}^{-2}$  white light for 12 hours, followed by 12 hours of darkness. The obtained data revealed an open circuit voltage (OCV) value of approximately 150 mV when the effects of photocatalysis were ignored. Notably, there was a difference of around 240 mV in the open circuit voltage measurements between dark and light environments. As a result, a simple, self-sustainable, biocompatible, and eco-friendly energy-harvesting 3D bio-anode embedded BPV cell device was developed using a CNF/alginate scaffold and had high power outputs relative to similar studies (Table 1). This innovative approach leads to the generation of bioenergy with the potential of causing a substantial impact on futuristic energy-generation systems, which could serve as a viable alternative for eco-friendly energy systems for point-of-care (POC) diagnostics and portable electronics. POC diagnostics are critical for detecting several diseases rapidly and efficiently both in developed and low-income countries. However, energizing them sufficiently in low-income countries is a main obstacle since the electricity grid is not well-established, and battery usage is not cost-effective.<sup>60</sup> Hence, self-sustainable power sources such as cyanobacteria-based BPVs that can be integrable to lab-on-a-chip have a crucial role in POC diagnostics to operate them autonomously under challenging environmental conditions.<sup>18</sup> In addition, these power systems can be utilized as portable electronic devices by connecting several 3D bio-anode scaffolds in serial and parallel

**Table 1** Comparison of the results with the literature. Only the upper surface area of the scaffold structure is provided since comparisons were made with two-dimensional systems. Although light will still penetrate the interior regions of the scaffold, the active site will exist solely on the surface due to bacterial activation and consequent color change in the structure

Species	Anode properties: material, area	Peak power density	Ref.
<i>Synechocystis</i> sp. PCC 6803	Carbon nano tube 28.4 $\text{cm}^2$	$0.38 \pm 0.07 \text{ mW m}^{-2}$	39
<i>Synechocystis</i> sp. PCC 6803	PEDOT: PSS/DMSO 0.503 $\text{cm}^2$	$10.7 \mu\text{W cm}^{-2}$	61
<i>Synechocystis</i> sp. PCC 6803	PEDOT: PSS on carbon cloth 0.385 $\text{cm}^2$	$43.8 \mu\text{W cm}^{-2}$	18
Algal strains CC-125 wild-type mt + [137c]	Aluminum sputtered gold 4.84 $\text{cm}^2$	$1914 \text{ mW m}^{-2}$	62
<i>Synechocystis</i> sp. PCC 6803	InBiSn alloy 0.03 $\text{mm}^2$	$100 \text{ mW m}^{-2}$	63
<i>Synechococcus</i> sp. WH 5701	ITO-PET 12.56 $\text{cm}^2$	$10.3 \text{ mW m}^{-2}$	64
<i>Chlorella vulgaris</i>	Carboxymethylated cellulose nanofiber-alginate sheet 22.4 $\text{cm}^2$	$1.9 \pm 0.13 \text{ W m}^{-2}$	21
<i>Synechocystis</i> sp. PCC 6803	CNF/Alginate hydrogel 3.14 $\text{cm}^2$	$0.0534 \text{ W m}^{-2}$ or $53.4 \text{ mW m}^{-2}$	This Study



to increase the power output to energize electronic devices. Thus, this innovative approach leads to the generation of bioenergy with the potential of causing a substantial impact on futuristic energy-generation systems, which could serve as a viable alternative for eco-friendly energy systems.

## 2. Materials and methods

### 2.1. Materials

The chemicals used in this study were purchased from Sigma Aldrich (USA), Nanografi (Türkiye), Alfa Aesar (USA), and Krayden (USA). *Synechocystis* sp. PCC 6803 Strain (original isolation from Berkeley, California) was purchased from Phycotec, Türkiye. BG-11 broth (100× concentrate), Hydrazine Hydrate, Nafion 117, dimethylacetamide (DMAc), and polyvinylidene fluoride (PVDF) powder were acquired from Sigma Aldrich. Cellulose nanofiber (CNF), graphene oxide water dispersion (8 mg mL<sup>-1</sup>), and conductive carbon powder (30 nm) were obtained from Nanogafi. Polydimethylsiloxane (PDMS), PDMS curing agent, and poly (methyl methacrylate) (PMMA) were obtained from Krayden, while activated carbon (AC) powder was acquired from Kimyalab, Türkiye. Additionally, indium tin oxide (ITO) electrodes, which cover the bottom and the top surfaces of the 3D bioanode, were used to determine the internal resistance. They were purchased from Ossila with the following specifications: 100 nm thickness, resistivity of 20 Ω □<sup>-1</sup>, and surface roughness is 1.8 nm RMS (by AFM).

### 2.2. Methods

**2.2.1. 3D bio-anode fabrication.** The bio-anode structure was prepared by using CNF and alginate to constitute a 3D environment for cyanobacteria cells as shown in Fig. 2a. For this purpose, 4% wt of CNF and 4% wt of alginate powders were mixed in a 1:1 ratio using a BG-11 broth. The cells in the exponential phase (OD<sub>750</sub> = 1) were collected by centrifugation and added to the CNF/Alginate hydrogel structure. The prepared hydrogel and cell mixture was poured into a circular-shaped PDMS mold ( $r = 1$  cm,  $h = 0.4$  cm). The chemical crosslinking process was initiated by 1 Molar Calcium Chloride (CaCl<sub>2</sub>) at room temperature for 1 hour. After cross-linking, the excessive amount of CaCl<sub>2</sub> was removed, and the scaffold was placed in the central chamber of the BPV device.

**2.2.2. Air cathode fabrication.** Air cathode fabrication was performed to increase the gas exchange between the microfluidic BPV cell and the environment. The procedure was prepared in the light of the previous study as shown schematically in Fig. 2b.<sup>65</sup> Briefly, PVDF powder was dissolved in *N,N*-dimethylacetamide (DMAc) by stirring at room temperature for 8 hours until the complete dissolution was achieved. Then, (10%) PVDF/AC/CB (30:3:10) solution was prepared according to 8.8 mg cm<sup>-2</sup> AC loading. The obtained mixture was spread through the stainless-steel mesh. To promote the phase inversion, the obtained air cathode was placed into deionized (DI) water at room temperature for 15 minutes, and the cathodes

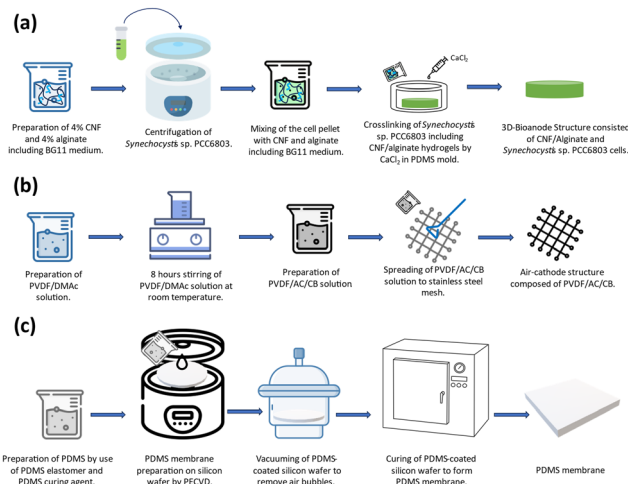


Fig. 2 The fabrication process of (a) 3D-Bioanode composed of CNF/alginate and *Synechocystis* sp. PCC 6803. (b) Air-cathode consisting of PVDF/AC/CB. (c) PDMS membrane.

were dried in a laminar hood for >6 hours and stored in DI water.

**2.2.3. PDMS membrane preparation.** The transparent and porous nature of PDMS makes it special to be utilized in many biological applications. The process of PDMS membrane preparation is displayed in Fig. 2c. Briefly, after the conventional cleaning procedure of the silicon wafer using acetone, isopropyl alcohol, and nitrogen drying, a 600 μm oxide layer was formed on a 4" (500 μm thick) silicon wafer using the plasma-enhanced chemical vapor deposition technique (PECVD) to easily remove the PDMS membrane after curing. Then, a mixture of PDMS base elastomer and curing agent prepared at a ratio of 10:1 was spun at 2000 rpm for 1 minute to spread smoothly on the SiO<sub>2</sub>-deposited wafer surface. Then, the wafer was vacuumed to remove the air bubbles inside the structure that were spread over the surface, and it was left to cure for 3 hours at 70 °C inside an oven to form a thin membrane. The resulting membrane thickness was measured as 20 μm (KLA tencor surface profiler). After the curing process, it was gently peeled off from the wafer surface to cover the top of the chamber where the scaffold was located.

**2.2.4. Inoculum of *Synechocystis* sp. PCC 6803.** *Synechocystis* sp. PCC 6803 was inoculated at 26 °C inside a 50 mL BG-11 medium that contained 1.5 g of NaNO<sub>3</sub>, 40 mg of K<sub>2</sub>HPO<sub>4</sub>, 75 mg of MgSO<sub>4</sub>, 36 mg of CaCl<sub>2</sub>, 1 mg of EDTA, and 6 mg of citric acid ferric ammonium citrate per 1 L of distilled water. During the inoculation of species, the shaker incubator was arranged at 120 rpm shaking under exposure to a white lamp for 2 weeks to procure photosynthesis. Finally, the growth of the species was monitored using a spectrophotometer device at an OD<sub>750</sub> value of 1.

**2.2.5. 3D bio-anode embedded BPV cell construction.** In our study, the microfluidic system houses a closed chamber. The bottom section includes an air cathode, while a platinum (Pt) electrode is placed on the upper section. The electrode, with its diameter immersed in the 3D bioanode, is enclosed by



a PDMS (polydimethylsiloxane) membrane at the top of the chamber. The design of the cylindrical microfluidic system was specifically tailored according to the bioanode. If the bioanode was shaped as a square prism or featured sharper edges, excessive distortion would have occurred at the corners during the curing process. Moreover, fabricating molds with sharp edges poses greater challenges compared to cylindrical structures. As a result, a cylindrical geometry was chosen. The difference in the design of the inlet and outlet microfluidic channels aims to facilitate a consistent fluid flow. A wide inlet channel paired with a narrower outlet channel would impede the exit of the fluid from the chamber, disrupting the desired flow. Conversely, a narrower inlet channel allows the fluid to gradually fill the chamber and then slowly exit through the outlet channel positioned at the top of the cylindrical chamber. This configuration ensures a consistent flow, supports systematic measurement progress, and minimizes variations in the experimental results. The choice of a PDMS chamber stems from the ease of processing, rapid production capabilities, and biocompatibility of PDMS compared to other materials.

A schematic of a 3D bio-anode embedded BPV cell unit is shown in Fig. 3. The developed BPV cell is composed of the following parts: two thick poly (methyl methacrylate) (PMMA) plates, holding the whole structure together, 3 PDMS structures peeled off from the molds, a polydimethylsiloxane (PDMS) gas permeable membrane, a 3D bio-anode structure, a proton exchange membrane (PEM) made of Nafion membrane and an air cathode. We used 3D printed models as a mold to fabricate the PDMS microfluidic channel, which has an inlet ( $300\ \mu\text{m} \times 300\ \mu\text{m}$ ), an outlet ( $2\ \text{mm} \times 2\ \text{mm}$ ) channel, and a large hole (with a 2.1 mm diameter that holds the 3D bio-anode inside). The total thickness of each PDMS layer is 4 mm. Biocompatible structures were obtained by utilizing the PDMS elastomer base and curing agent mixed at a ratio of 10 to 1 after vacuuming and curing at  $70\ ^\circ\text{C}$  for 3 hours. We designed the outlet channel to be larger than the inlet because of flow conditions and sandwiched all PDMS parts to serve as a BPV unit. The thick PMMA layers, which were fabricated using the computer numerical control (CNC-controlled) laser cutting method, are the exterior materials that hold all structures together with the

use of screws. It has three essential holes: inlet, outlet, and bacterial inoculation chamber. After the preparation of PEM and an air cathode, we assembled each part, including the 3D bio-anode structure and platinum electrode (Section S1, ESI<sup>†</sup>), and utilized the BG-11 medium as a catholyte.

During the experiments, the distance between the electrodes was set to  $\sim 2\ \text{mm}$ . The total thickness of the scaffold is 5 mm, and a platinum electrode was inserted inside the bioanode (3 mm deep) (This information is detailed in Section 2.2.9. Effective electrode area). At the bottom, there is a planar (coated on meshed stainless steel) air cathode electrode, and the total gap between the air cathode and the Pt electrode is around 2 mm.

**2.2.6. Electrical characterization of 3D bio-anode embedded BPV cell unit and illumination.** Power overshoots and voltage reversal issues are common problems in biofuel cells that cause poor performance, and the calculation of maximum power density is challenging.<sup>66</sup> Thus, it is required to seek approaches to calculate the internal resistance without facing power overshoot and voltage reversal. One method involves the electrode potential slope analysis. It provides a reliable ohmic  $R_{\text{int}}$  value, which includes solution resistance, contact resistance, and cell resistance. This method leads to a different value of the internal resistance. For this reason, we applied electrochemical impedance spectroscopy (EIS) in closed circuit mode and 2 electrode techniques using a potentiostat (PARSTAT MC, Princeton Applied Research, USA) with a graphical user interface in VersaStudio 2.63.3 version. However, due to the power overshoot and voltage reversal in the low external resistances, this process was managed by connecting a high-resistance load. Furthermore, hybrid pulse power characterization (HPPC) testing is a method for determining the power densities of BPV cells.

Temperatures higher than  $27\ ^\circ\text{C}$  induce the demise of bacteria so it became imperative to employ illumination at the most minimal feasible intensity. To achieve this objective and forestall heat generation within the experimental configuration during the characterization process, a meticulous strategy was devised. Specifically, the LED lamp, serving as our source of white light, was positioned at a distance of 12 cm above the bioanode. Furthermore, a stringent protocol was implemented to maintain the incident light on the bioanode surface at a precisely controlled luminance level. Then, we started to measure the harvested energy from the bioanode as the open circuit voltage using a voltmeter.

Open circuit voltage provides information about the electrical properties of BPVs under light and dark situations, which depends on the active area of the scaffold illuminated with white light in this study. The open circuit voltage of BPV was measured with a voltmeter without connecting to an external load (Section S2, ESI<sup>†</sup>).

Cyanobacteria can initially be cultured under white light to accumulate sufficient biomass and then under colored light to increase phycobiliprotein production.<sup>67</sup> Since white light encompasses various wavelengths, its use also ensures adequate energy generation. The intensity and duration of light exposure are crucial for the photosynthetic activity and energy

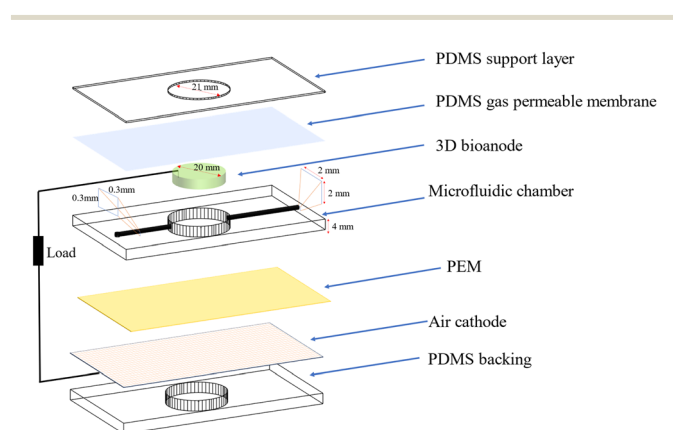


Fig. 3 Layer-by-layer design for 3D Bio-anode embedded BPV cell unit.



generation in BPV systems. Variations in light/dark cycles can significantly impact photosynthesis and nitrogen fixation rates in cyanobacteria, thereby influencing the overall efficiency and power output of the system.<sup>68</sup> At the same time, the use of white light is important due to the system which we developed and allows the use of energy directly from the sun. If we needed a specific wavelength and light outside that wavelength, it would have harmed the biota and would have required additional equipment and increased costs. This study suggests that the developed system could be integrated into small-scale electronic systems to power them on sunny days.

**2.2.7. Bacterial fixation and SEM imaging procedure.** The morphology of the 3D bio-anode compartment was characterized using the scanning electron microscopy (SEM) technique. For this purpose, a 4% glutaraldehyde solution was used for treating the 3D bio-anode structure at room temperature for two hours. After fixation, the 3D bio-anode was washed with 0.1 M phosphate buffer saline (PBS) three times. Then, 30%, 50%, 70%, 80%, 90%, 95%, and 100% of ethanol solutions were prepared, and the 3D bio-anode scaffold was dehydrated for 5 minutes each.

**2.2.8. Confocal microscopy imaging of 3D bio-anode structure.** To monitor the *Synechocystis* sp. PCC 6803 seeded CNF/alginate bio-anode compartment, in micro-meter range confocal microscopy was implemented. Fluorescence image data were acquired using the Zeiss LSM 710 laser scanning confocal microscope to monitor cellular proliferation and morphology of the *Synechocystis* sp. PCC 6803 after 15-day cultivation.

**2.2.9. Effective electrode area.** In the pursuit of internal resistance assessment, the electrochemical impedance spectroscopy (EIS) method was executed, which entailed the strategic placement of ITO electrodes possessing congruous surface area and conductivity attributes, on both facets of the bioanode. Subsequently, these measurements were rigorously modeled *via* an equivalent circuit to determine the internal resistance value. The surface dimensions of the ITO electrodes remained congruent at precisely 314.16 mm<sup>2</sup>. However, in the context of the open-circuit and closed-circuit evaluations, a platinum electrode was inserted 3 mm inside the bioanode, boasting a minuscule diameter of 0.5 mm, which served as a counterpart to the air cathode. It should be noted that the air cathode's surface area was 314.16 mm<sup>2</sup>, in stark contrast to the modest accessible surface area (9.621 mm<sup>2</sup>) of the platinum electrode. However, since the electrode touched both surfaces of the scaffold, and the measurements were made in this fashion, the total effective area should have been twice the obtained value and was taken as 628.32 mm<sup>2</sup> (0.00063 m<sup>2</sup>) in the calculations.

## 3. Results and discussion

### 3.1. Performance evaluation of a 3D bio-anode embedded BPV cell unit

To assess the effectiveness of electricity-generating devices, it is essential to have information about fundamental parameters such as open circuit voltage and internal resistance in order to determine the generated power.

**3.1.1. Open circuit voltage measurements of a 3D bio-anode embedded BPV cell unit.** In this section, we performed open circuit voltage measurements, which is the most common electrical measurement technique used for testing electricity-generating devices without connecting them to any load, (Fig. S3, ESI<sup>†</sup>). Accordingly, cyanobacteria behaved differently under light, illuminated by a 16.7 W m<sup>-2</sup> white light source, and in a lightless environment, which can be seen in the open-circuit voltage measurements shown in Fig. 4a. The open circuit voltage has negative values in light and positive values in the dark, which is associated with linear electron transfer. According to the classical linear electron transport mechanism explained by Lea *et al.*,<sup>69</sup> which is shown schematically in Fig. 5, when chlorophyll is excited, its redox potential becomes highly negative (−0.6 V), making it function as an electron donor. Once oxidized, the chlorophyll returns to its redox potential (+1.3 V), which is positively charged and attracts electrons from water. Thus, it can be stated that the initial uneven distribution of bacteria on the scaffold caused higher power generation in the absence of light. However, on the fourth day, the excitation of chlorophyll by light led to a reduction in positive voltage values and an increase in negative values, Fig. 4b. This indicates that the bacteria could have successfully reached the most mature size and are now uniformly distributed throughout the scaffold. The excited electron then passes from the reaction center through a sequence of cofactors until it eventually reduces plastoquinone (PQn), which is a type of benzoquinone serving as a primary electron carrier in the photosynthetic tissues of cyanobacteria. The electron carrier is able to move through the hydrophobic membrane due to its solubility in lipids. Within the PSII, which behaves as a proton pump, two excited electrons are transferred to PQ, which is adequate for reducing plastoquinone to plastoquinol (PQH<sub>2</sub>), and the PQn takes in two protons from the cytoplasmic side of the thylakoid membrane. Upon the excitation of the reaction center four times, enough electrons are transferred to reduce two molecules of PQn, remove four protons

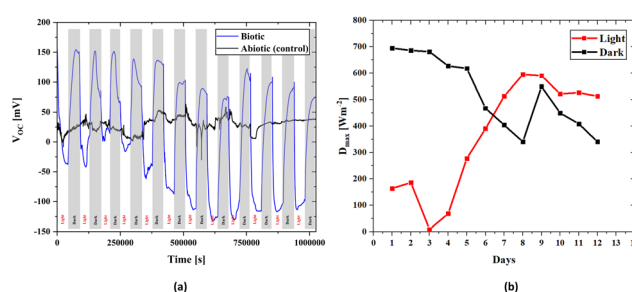


**Fig. 4** Long-term open circuit voltage results of the scaffold with bacteria and without bacteria under 12 hours of light, provided by a 16.7 W m<sup>-2</sup> white light source, and 12 hours of dark conditions. (a) The graph demonstrates two different measurement results; the black line indicates the open circuit voltage measurement result of the empty scaffold structure without bacteria (with a platinum wire anode and an air cathode). The cyclic blue curve shows the open circuit voltage measurement result of the bacterial scaffold (with a platinum wire anode and an air cathode). (b) Observation of the change in maximum power densities of the biotic scaffold over time under light and dark conditions.





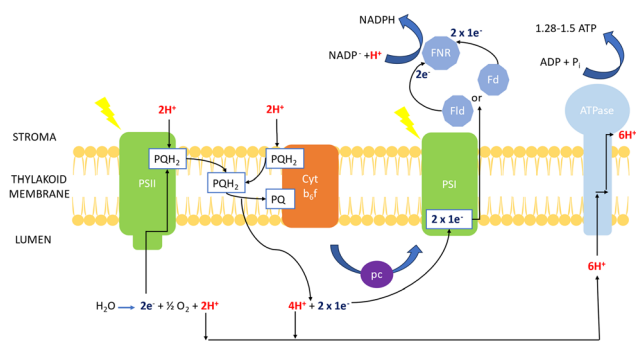


Fig. 5 Mechanism of photosynthesis in chlorophyll of cyanobacteria (based on transport mechanism explained by Lea *et al.*<sup>69</sup>).

from the cytosol, and extract four electrons from two water molecules, which produces O<sub>2</sub> and four protons in the lumen. Hence, PSII serves as a proton pump with the net transition of protons through the lumen from the cytosol.

The electron excitation and donation in PSI to other cofactors have similarities to PSII. Herein, there is electron transport to ferredoxin (Fd) on the cytosolic side of PSI from H<sub>2</sub>O at the luminal part of PSII by interchain components.<sup>70</sup> Electrons are donated from Fd to NADP<sup>+</sup> via Fd-NADP<sup>+</sup> oxidoreductase (FNR). Furthermore, the flow of H<sup>+</sup> through the thylakoid lumen due to the electron transport between PQ and the Cyt b<sub>6</sub>f creates a proton motive force, which consists of both electric field ( $\Delta\psi$ ) and concentration ( $\Delta\text{pH}$ ) gradients obtained to produce ATP by ATPase.

There is an apparent difference when comparing the open circuit voltages of bacterial cultured and abiotic scaffolds in Fig. 4. In the biotic structure, there are changes in the open circuit voltage due to light sensitivity. Still, in the abiotic form, there is no light sensitivity. However, there are instantaneous changes due to the liquid flow and charge transfer resistance on the electrode surface due to molecules inside the fluid. Thus, the control measurement confirms that the BPV system is working properly. At open circuit voltage, there seems to be a stability problem within the first four days that could be related to the number of the bacteria inside the scaffold and the adaptation of the bacteria to the environment. After a short time, the electrical measurements stabilize on both the positive and negative axes. Thus, the increase in the bacterial population over time also suggests that it behaves in accordance with the classical linear electron transport mechanism, which demonstrates light dependence on OCVs. In the control measurement, the voltage value is around 30 mV, which is due to the difference between the anode and cathode electrode potentials and molecular excitations inside the fluid.

The efficiency of microbial fuel cells (MFCs) and BPVs is affected by several factors such as activation overpotentials, ohmic losses, and concentration polarization.<sup>71</sup> These factors are considered in micro-size MFCs using special electrodes with physically or chemically modified surfaces *via* specified materials.<sup>71</sup> Similar to natural or artificial electron transfer agents that can easily participate in the redox reactions of

biological components,<sup>71</sup> electrodes also have different redox potentials which can directly contribute to the generated potential.<sup>72,73</sup> To eliminate the redox potential of materials, an abiotic scaffold is used as a reference potential to determine the voltage output during biotic situations. Thus, the selection of anode and cathode materials gains importance. The function of the air cathode reduces the cathodic resistance by increasing the amount of dissolved oxygen,<sup>58</sup> and the Pt anode material is a nonreactive material for the BPV system which can contribute to the current collection mechanism and complete the circuit by connecting a load.

Although *Synechocystis* sp. is promising because of its ability to perform photosynthesis, the oxygen it generates might disrupt the functionality of bioelectrochemical systems. The release of oxygen by *Synechocystis* sp. during photosynthesis interferes with the electron uptake by the bio-anode, causing decreased effectiveness in electron harvesting and diminished power output which occurs due to the natural tendency of *Synechocystis* sp. to utilize electrons for their own metabolic processes.<sup>74</sup> This problem poses a considerable obstacle in the optimization of bioelectrochemical systems that leverage photosynthetic microorganisms. In addition, the release of oxygen by *Synechocystis* sp. might lead to the generation of reactive oxygen species (ROS), potentially triggering damage to both the biological and electrochemical components within the system.<sup>75</sup> Therefore, current studies aim to advance various strategies to improve the electron capture efficiency in BPVs such as developing genetically modified strains of *Synechocystis* sp. to boost their electron transfer capabilities, optimizing the particular electrode materials and refining the design of bioreactors to increase the light absorption and energy conversion efficiency.<sup>16,74,76</sup>

Another difference between the 3D bio-anode embedded BPV cell and the other in the literature lies in the high voltage measurement when considering the redox potentials of the cyanobacteria under light or in dark hours. The solid 3D bio-anode structure has a larger internal resistance than 2-D bacterial cultures. For this reason, the calculation of internal resistance gains more importance.

**3.1.2. Internal resistance ( $R_{in}$ ) determination using EIS Technique.** The measurements of the pure internal resistance should be performed without incorporating the anode and cathode electrode resistances because they increase the internal resistance of the bulk structure. First, we used the open circuit EIS technique with fully oxidized ITO electrodes and continued to determine the internal resistance of the scaffold using Pt/Air cathode electrodes. However, we can state that the internal resistance should be measured using a bulk electrode, which is connected to the surface of the scaffold. In the Pt/Air cathode configuration, the platinum wire affects the conductive path due to insertion inside the scaffold body. Thus, the most effective method to determine the internal resistance for the open circuit EIS technique is utilizing similar electrodes for the anode and cathode side. First of all, the internal resistance was determined using the impedance data equivalent circuit model obtained from the open circuit EIS technique using ITO





electrodes (Section S4A, ESI<sup>†</sup>) in the range of 1 MHz to 100 Hz with a 10 mV signal amplitude. According to our results, a scaffold internal resistance of 174.4  $\Omega$  was determined.

Another technique for determining the internal resistance value is the scanning EIS technique. Here, we used Pt/air cathode electrodes, which are commonly used in standard measurements for both biotic and abiotic systems, which were implemented by connecting BPV to various external resistances to find the total internal resistance ( $R_{\text{int}}$ ) of the cell, including electrode resistances (Fig. 6). This approach aimed to minimize measurement errors. The obtained results were analyzed to determine the internal resistance and understand the influence of electrode potentials on the total system. The impedance spectroscopy (EIS) was conducted across a frequency range of 1 MHz to 100 Hz with a 10-mV signal amplitude. The overall internal resistance ( $R_{\text{int}}$ ) consisting of the charge transfer resistance ( $R_{\text{ct}}$ ) and solution resistance ( $R_{\text{s}}$ ) is affected by the external resistance, and it exhibited a tendency to decrease as the external resistance decreased which agrees with Kim's study.<sup>66</sup>

We obtained a total internal resistance of 67.7  $\Omega$  in the open circuit mode and 92.8  $\Omega$  when using the scanning EIS technique (Section S4B and C, ESI<sup>†</sup>). The difference in internal resistances between the open-circuit and closed-circuit models occurs due to the length of Pt inside the scaffold and the resistance effect in the closed-circuit model. According to Kim's approach,<sup>66</sup> an increase in the external resistance results in a decrease in the current value which leads to less electron movement and reduces the number of ion generation in the whole system. This directly affects the value of the internal resistance, in other words, when the ion density increases, it leads to an increase in charge movement within the system, thereby boosting the conductivity and causing a reduction in the internal resistance.

As seen in Fig. 6b, abiotic scaffolds were utilized to determine the internal resistance. The main difference between the two results is the change in the solution resistance and a significant gap between their charge transfer resistances. The primary difference in the case of Pt/air cathode electrodes is

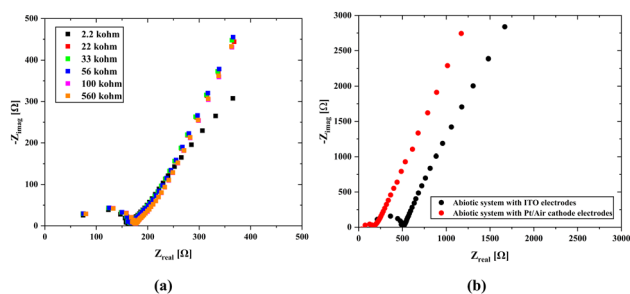


**Fig. 6** Comparison of EIS measurements of abiotic systems. (a) The results of the tests performed with the scanning EIS technique using the Pt/Air cathode electrode system in the abiotic system. In this part, resistors of 2.2 k $\Omega$ , 22 k $\Omega$ , 33 k $\Omega$ , 56 k $\Omega$ , 100 k $\Omega$ , and 560 k $\Omega$  were used, respectively. (b) Impedance measurements with the open circuit method using Pt/Air cathodes and ITO/ITO electrodes in the abiotic system and comparison of the results.

that the platinum wire was inserted through the scaffold body. Since this shortens the mean free path, which is the passage of ions from one electrode to the other, a decrease in the internal resistance might have been caused. On the other hand, the material properties used in the air cathode allow for the transfer of more ions to the structure, which can cause a significant increase in ion movement. In the case of ITO electrodes attached on both surfaces, since the electrode potentials will cancel each other, it will be easier to obtain information about the internal resistance of the solid scaffold (abiotic) structure through which the nutrient fluid flows. At the same time, due to the transparency of ITO, it can also be used under light. However, since ITO was coated on the glass surface with a thickness of 100 nm, it is not possible to use it in the biotic system as there would be no carbon dioxide and oxygen transition.

A consistent nutrient flow and stable environmental conditions lead to rapid growth of the bacterial population in the hydrogel scaffold. Our microfluidic channels were designed to evenly distribute nutrients throughout the scaffold and to efficiently remove waste by emptying once the chamber is full, thereby ensuring a balanced nutrient supply. The effluent turned green within just a few days which marks a significant increase in the bacterial population and demonstrates the normal operation of our system. Impedance measurements were also made over time to monitor any changes in the system. Here, it was foreseen that the bacterial population would dominate the scaffold structure over time, which would cause a change in the internal resistance and create a biofilm layer on the electrode surfaces, leading to an increase in  $R_{\text{int}}$ . However, as seen from the open circuit EIS measurements (Fig. 7-a), the effect on the internal resistance is negligible, and a slight increase in the charge transfer resistance occurs over time. When the results are evaluated, it can be observed that the properties of the biotic structure preserve their stability over time.

There is a change in the charge transfer resistance rather than the internal resistance in the impedances of the biotic and abiotic systems (Fig. 7b) evaluated under the same conditions. This is because of the possibility of double-layer capacitance formation on the electrode surfaces originating from cyanobacteria, which may be due to the formation of biofilms on the

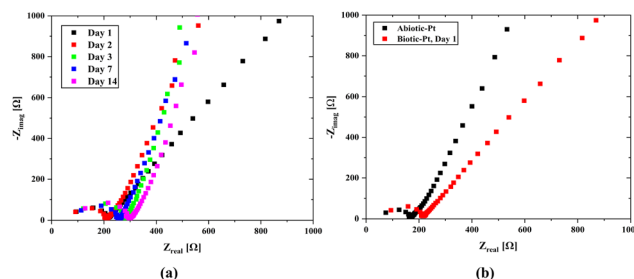


**Fig. 7** EIS results of biotic and abiotic systems in the range of 1 MHz to 100 Hz with 10 mV signal amplitude. (a) Daily potentiostatic EIS results of the biotic scaffold with Pt/air cathode electrodes. (b) Potentiostatic EIS results of biotic and abiotic scaffolds with Pt/air cathode electrodes.



electrode surfaces originating from bacteria. The characteristics of the anode surfaces hosting microbial communities in BPV systems impact the electrochemical charge transfer rate at the electrode by altering the kinetics of metabolic reactions in the biotic compartment.<sup>17</sup> The large surface area of the 3D scaffold-based bio-anodes can enhance the mass transfer of the nutrients and reaction kinetics, thereby maximizing the power outputs of the BPVs.<sup>77</sup> However, the charge transport to the electrode surface becomes challenging, and a decrease in power capacity could occur. The internal resistance (Section S4, ESI†) was determined using the abiotic scaffold with ITO–ITO electrodes to be 174.4  $\Omega$ , while it was 103.7137  $\Omega$  in the biotic system with the Pt/air cathode electrode configuration. It can be clearly seen that there is a slight change in the internal resistance due to the bacterial effect. At the same time, for the abiotic scaffold, the internal resistance was found to be 67.7  $\Omega$  when the Pt/Air cathode electrode configuration was used in the open circuit mode while it was 92.8  $\Omega$  when implementing the scanning EIS technique. It should be noted here that in the biotic system, the additional resistance due to the bacteria presence must be included in the system. This was directly reflected as an increment in the internal resistance, which was obtained as 103.7  $\Omega$ . In the evaluation of power density, we used 174.4  $\Omega$  for the internal resistance.

Here, it should be also noted that the use of Pt wire in a Pt/air cathode configuration might potentially disrupt the current path within the scaffold (3D bioanode) and affect the measured internal resistance. The platinum wire might change the distribution of current flow and introduce additional resistances or conductive pathways that were not present in the original configuration. Thus, it can lead to inaccuracies in measuring the internal resistance of the scaffold as the Pt wire itself might have different electrical properties compared to the scaffold material. However, since the Pt wire only serves as a current collector and has a high conductivity, it will not have any function other than providing the connection between the scaffold and the measuring device. Therefore, the resistance of the Pt wire could be ignored when compared to the internal resistance of the scaffold.

We tested different configurations of electrode connections to determine the real internal resistance of the scaffold and the 3D bioanode to compare the effects of the surface areas of the electrodes on the internal resistance. ITO surfaces completely cover the scaffold surface which could be the best model for measuring the internal resistance; however, it blocks gas permeation through the scaffold and could potentially disrupt the biota. Regarding the use of Pt electrode and air cathode, the significant difference in the surface area between the platinum counter electrode and the air cathode in biophotovoltaic systems arises from the reaction kinetics, material considerations, and optimization of the system design.<sup>78</sup> The air cathode, which facilitates the oxygen reduction reaction (ORR), requires a larger surface area to maximize the efficiency. This larger area provides more active sites for the ORR, thereby boosting the overall performance and efficiency of the biophotovoltaic system. In contrast, the platinum counter electrode primarily

functions as a reference or balancing electrode to complete the electrical circuit. Thus, it can be stated that its role is less dependent on the surface area since it typically supports the oxidation reaction with a high-activity catalyst, even on smaller surfaces.

A smaller counter electrode can restrict current flow and hinder the overall performance of the electrochemical cell.<sup>79</sup> This occurs because a reduced surface area increases the internal resistance, which may not accurately reflect the cell behavior under standard conditions. Therefore, using a counter electrode with a sufficiently large surface area is crucial for precise performance measurements. However, platinum electrodes are not transparent and inhibit the diffusion of gases such as carbon dioxide and oxygen. A 3D bioanode, if fully closed by metal electrodes at the bottom and the top sides, will lack sufficient light penetration and carbon dioxide diffusion, impairing photosynthesis and reducing power generation. Consequently, further innovation is needed to design a smaller 3D bioanode with a mesh structure that allows better system utilization.

**3.1.3. Power density evaluation.** Cyanobacteria are photosynthetic organisms capable of converting light energy into chemical energy through photosynthetic activity.<sup>39,80</sup> When these bacteria absorb light energy through chlorophyll and other pigments, electrons are elevated from their ground state to a higher energy level.<sup>81</sup> These high-energy electrons are then moving through the photosynthetic electron transport chain,<sup>82</sup> generating chemical energy in the form of ATP and NADPH.<sup>81</sup> Additionally, some of the high-energy electrons are transferred to the outer membrane of the cell, creating an electrical current flow and producing a voltage between the electrodes of the BPV cell. This transfer results in power generation (Power = Voltage  $\times$  Current). The observed voltage changes in the cells are directly related to the photosynthetic activity of the cyanobacteria and the efficiency of electron transfer to the electrode. Therefore, the voltage combined with the current from the electron flow determines the actual power production in the BPV cell.

The 3D BPV system developed in this study can generate energy in light and dark environments. As shown in Fig. 4, the change in the voltage values to either a positive or negative value depends on the environment, and the power value is provided for both scenarios. To assess the power densities, we first determined the maximum value of the voltage for every 12-hour light and dark conditions. The voltage ( $V$ ) and current density ( $J$ ) are used to obtain the power density ( $P$ ). Current density is the current per unit area, while power density is calculated as the product of voltage and current density. A change in voltage suggests that there is a change in the electrical potential difference in the system, which can affect the current flow and power density. Here, Fig. 4a presents the change in voltage outputs of the biotic system in light and dark environments every 12 hours. Fig. 4b includes the power density values calculated from the maximum value of the voltage obtained from Fig. 4a for every 12 hours (light and dark). The 3D bioanode internal resistance value was obtained



using the internal resistance, which directly reflects the power density values since the impedance values are assumed to be constant daily. Moreover, the maximum power density was determined (Section S5, ESI<sup>†</sup>) by utilizing the internal resistance value of  $0.1096 \Omega \text{ m}^2$ , which was the biotic internal resistance of the scaffold, in both evaluations, and the change in maximum power densities during days is schematized in Fig. 4b.

According to the maximum power transfer theorem,<sup>83</sup> which is valid in both alternating current (AC) and direct current (DC) circuits, when the impedances of the load connected to the source and the source's internal resistance are equal, the maximum power transfer from the source to a load is achieved. Accordingly, when a suitable load is connected to a source with a known internal resistance, the load will operate at the maximum performance. In the first days of culturing bacteria to the bioanode, the maximum power was calculated to be  $0.0534 \text{ W m}^{-2}$  for dark hours and  $0.03911 \text{ W m}^{-2}$  for light hours. The reason for the lower power generation due to the photosynthesis effect in the light environment is related to a slight increase in the internal resistance value (Fig. 7b). However, the maximum open circuit voltages were higher in light hours than dark hours after some days, Fig. 4b, and it directly affects the maximum power densities. Therefore, we can clearly see that even though the higher power was obtained in the lightless environment, this situation reversed over time, and the power obtained in the lighted environment increased. Although the considerable reduction in the transmittance of the light through the scaffold (Section S6, ESI<sup>†</sup>) causes more open circuit voltage in the dark environment that occurs in the early stages of bacterial growth, the growth of bacteria in all parts of the scaffold over time indicates that not only the effect of light but also nutrition and ambient temperature are effective in the proliferation of bacteria. It can be stated that after a few days when the electricity generation is higher in the light environment than in the dark environment, the chlorophyll activation amplifies, contributing to the electricity generation of the bacteria. Although light transmittance is a disadvantage of the 3D scaffold-based BPVs, keeping bacteria together in a 3D environment and being a healthy nutrient medium are effective features of this structure.

Another major parameter is the efficiency of converting the incoming light into electrical energy, which is determined by dividing the output power density by the power density of the entering light (Section S7, ESI<sup>†</sup>). The illuminance of the light used during the experiments was measured to be  $16.7 \pm 0.1 \text{ W m}^{-2}$  (Section S7a, ESI<sup>†</sup>). The maximum power density of the 3D bioanode was calculated to be  $0.0534 \text{ W m}^{-2}$ . The conversion efficiency was calculated (Section S7b, ESI<sup>†</sup>) to be 0.32%, which is high for a new generation 3D bioanode structure and thus will open a new lane for future power generation studies.

Identifying time constants in this process allows us to obtain power density values through experiments. The PARSTAT PMC 1000 computer-controlled potentiostat was used to record polarization curves at room temperature in a two-electrode

(air cathode/Pt) electrochemical cell. Reliable results were obtained with ease, allowing for confident analysis and interpretation of data. The biotic scaffold structure was subjected to HPPC testing at separate times in the dark and under light. Current density and power density values *versus* open circuit voltage are provided in Section S7c (ESI<sup>†</sup>). The absolute maximum power density obtained in the dark, and the maximum power density obtained under light had close values ( $0.08 \text{ W m}^{-2}$ ). The negative result regarding the maximum power densities in measurements taken under light is due to the negative open circuit voltage. Also, the light caused an increase in electron transfer, which directly led to higher negative values in the current density which can be seen in the cyclic voltammograms in Section S8 (ESI<sup>†</sup>).

### 3.2. Image analysis

**3.2.1. Results of scanning electron microscopy (SEM) analysis of the 3D bio-anode structure.** Fig. 8 displays the SEM images of the 3D bioanode structure as a reference without the *Synechocystis* sp. PCC 6803 strain (Fig. 8a) and proliferation of *Synechocystis* sp. PCC 6803 strain inside the 3D bioanode structure (Fig. 8b and c). The reference hydrogel scaffold having only sodium alginate and CNF does not show clear structures since the drying process affected its morphology. However, there are some fiber-like textures that might belong to CNF. The source of the CNF which is utilized for the bio-anode structure is cotton with an average particle size of 10–20 nm wide and 2–3  $\mu\text{m}$  long. CNF is a hydrophilic material, and its surface contains both hydroxyl and carboxyl groups which enable its functionality.<sup>84</sup> Crosslinking of CNF and alginate by a multivalent metal cation,  $\text{CaCl}_2$ , is a common technique to obtain hydrogel formations and exhibits unique microstructures like bundles.<sup>85,86</sup> The concentration of  $\text{CaCl}_2$  is a critical factor that affects the mechanical properties of a hydrogel. Besiri *et al.*<sup>87</sup> indicated that higher concentrations of  $\text{CaCl}_2$  in a low volume form strong networks in a hydrogel whereas the lower cation concentrations at higher volumes result in weaker gels. Crosslinking time is another factor affecting the water content of the hydrogel where the calcium ions density in the hydrogel environment is changed.<sup>88</sup> Herein, a greater abundance of calcium ions in the hydrogel network can promote the stability of hydrogels due to remaining less space for water molecules, thereby resulting in reduced dehydration. In the current study, the high molarity of  $\text{CaCl}_2$  (1 M), short

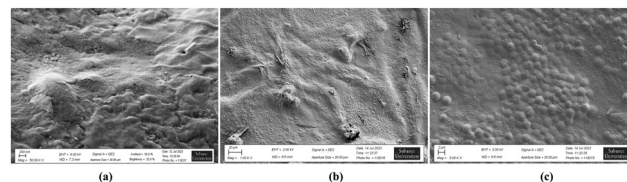


**Fig. 8** Results of SEM analysis for 3D bioanode structure (a) reference, only sodium alginate, and CNF hydrogels. Scale bar – 200 nm. (b) *Synechocystis* sp. PCC 6803 seeded bioanode structure, scale bar – 20  $\mu\text{m}$ . (c) *Synechocystis* sp. PCC 6803 seeded bioanode structure, scale bar – 2  $\mu\text{m}$ .





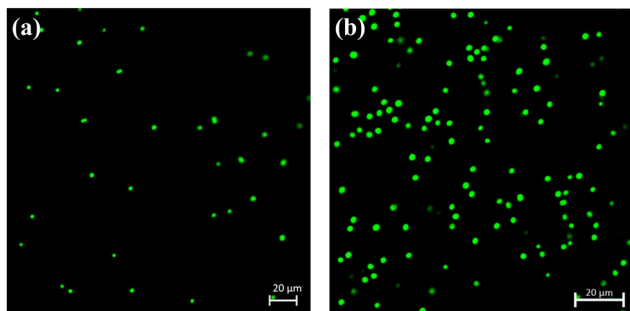


Fig. 9 Results of confocal microscopy analysis for (a) *Synechocystis* sp. PCC 6803 culture, scale bar -20  $\mu\text{m}$ . (b) *Synechocystis* sp. PCC 6803 seeded 3D bio-anode structure, scale bar -20  $\mu\text{m}$ .

crosslinking time (1 hour) and low volume of  $\text{CaCl}_2$  (500  $\mu\text{L}$ ) have a significant impact on achieving a strong hydrogel network. Herein, Fig. 8b and c indicate that the strong hydrogel bio-anode structure greatly supports the proliferation and biofilm formation of *Synechocystis* sp. PCC 6803 without affecting their spherical shape morphology.

**3.2.2. Results of confocal microscopy analysis of 3D bio-anode structure.** In several studies, CNF and alginate materials have been employed for various applications of cyanobacteria such as ethylene production,<sup>89</sup> BPVs,<sup>21</sup> and hydrogen production.<sup>90</sup> The results of confocal microscopy analysis indicate that the developed CNF/Alginate hydrogel scaffold promotes cellular proliferation of *Synechocystis* sp. PCC 6803 (Fig. 9-a). Morphological changes in cyanobacteria affect the electron transfer rates and thus electricity generation.<sup>91</sup> In our scaffold, the seeded cells do not exhibit any morphological changes since PCC 6803 in both groups, A and B, have a spherical shape and an average diameter of 2  $\mu\text{m}$  (Fig. 9a and b) which implies that electron transfer rates are not interrupted.<sup>92</sup>

## 4. Statistical validation

In this study, a student's *t*-test was used to assess whether the light/dark conditions influenced biotic and abiotic groups based on their peak powers gathered from Section S7C (ESI<sup>†</sup>). A statistically significant difference ( $p$ -value = 0.0058 < 0.05) between group means would indicate a variation in the power density attributable to light or dark conditions, which is potentially linked to the biotic or abiotic nature of the samples. Detailed test results are presented in Section S9 (ESI<sup>†</sup>) – statistical analysis section.

## 5. Conclusion

In this study, we proposed a BPV cell unit with the ability of energy harvesting using a 3D hydrogel bio-anode, which embodies a cyanobacteria culture. The conversion of ATP into electrical energy was carried out in the chlorophyll of cyanobacteria which were seeded inside the 3D solid bio-anode structure where the necessary conditions were provided for their growth and reproduction. We examined the effects of

darkness and light on electricity generation. We utilized a 16.7  $\text{W m}^{-2}$  white light source and made open circuit measurements. For the abiotic 3D anode, the average voltage value obtained under light and dark conditions was around 30 mV, which varied at low values due to electrode potentials and different ionic effects caused by the continuous flow. In the biotic structure, positive (150 mV) and negative voltages (–125 mV) were observed under the influence of dark and light environments, which is due to the chlorophyll redox potential being negative and positive in the dark and light, respectively, as light stimulates chlorophyll. However, this situation reversed over time, and the open circuit voltage increased in the light environment and decreased in the dark environment. The peak power density (<0.08  $\text{W m}^{-2}$ ), another parameter used to assess the electrical characteristics of BPVs, was relatively higher compared to some of the other bioenergy-generating systems in the literature. Bacterial metabolism increases upon light exposure, so that a biofilm forms on the electrode surfaces, which eventually leads to an increase in the internal resistance and a subsequent decrease in the power density. Concurrently, as elucidated in the literature, augmenting scaffold characteristics to diminish resistivity by incorporating organic and biocompatible constituents or conductive particles within a more streamlined structure could precipitate a concomitant reduction in internal resistance, thereby directly amplifying power generation. Moreover, optimizing the composition of the 3D biofilm through a genetic algorithm could further enhance the photosynthesis efficiency and selection of superior species for cultivation within the scaffold could increase the performance. Additionally, enhancing the structural properties of the scaffold could improve the light penetration and nutrient distribution, as well as the electrical conductivity and surface area for biofilm growth. Lastly, refining the electrode design is crucial for increasing the energy-harvesting efficiency of the 3D biofilm. Our approach of generating bioelectricity from a 3D cyanobacterial biofilm, which was tested for the first time in the literature and developed as a proof-of-concept study, appears as a simple, efficient, and eco-friendly alternative, which paves the way for emerging applications such as new generation Lab-on-a-Chip systems. Therefore, in future studies, several 3D bio-anode compartments could be connected in serial and parallel configurations to increase the power output for scaling up the platform. In addition, the scaffold thickness must be decreased to reduce its internal resistance and to ensure the transfer of more light through the biofilm to increase power output. At the same time, tests could be performed to power LEDs or small electronic devices, and the concept could be utilized to self-power Lab-on-a-Chip applications.

## Author contributions

Z. M. and A. K. conceptualized the study. Z. M. and İ. B. collected data and drafted the manuscript. A. K. and G. G. supervised and critically revised the article, and all authors contributed to the technical content of the draft and motivated approval for the final version of the manuscript.



## Funding sources

This research was funded by the Turkish Academy of Sciences (TÜBA) in the framework of member research incentives.

## Ethics statement

The authors of the submitted article declare that the article's content does not require ethical committee approval and/or legal special permission.

## Data availability

The data could be obtained using the following link: [https://drive.google.com/drive/folders/1sTOFjlva7B4vNxP\\_rDI7c\\_94h4HGh3uY?usp=drive\\_link](https://drive.google.com/drive/folders/1sTOFjlva7B4vNxP_rDI7c_94h4HGh3uY?usp=drive_link).

## Conflicts of interest

There are no conflicts to declare.

## Acknowledgements

The gratitude for student support from the Faculty of Natural Sciences and Engineering of Sabancı University and Sabancı University Nanotechnology Research and Applications Center (SUNUM) is gratefully appreciated. This study was funded by the Turkish Academy of Sciences (TUBA) under the grant: Member Grant.

## References

- 1 Y. Liu, P. Cruz-Morales, A. Zargar, M. S. Belcher, B. Pang, E. Englund, Q. Dan, K. Yin and J. D. Keasling, *Cell*, 2021, **184**, 1636–1647.
- 2 H. Lee and S. Choi, *Lab Chip*, 2015, **15**, 391–398.
- 3 V. Singh, N. Singh, N. Tabassum and V. Mishra, in *Microbial Strategies for Techno-economic Biofuel Production*, ed. N. Srivastava, M. Srivastava, P. K. Mishra and V. K. Gupta, Springer, Singapore, 2020, pp. 249–264, DOI: [10.1007/978-981-15-7190-9\\_9](https://doi.org/10.1007/978-981-15-7190-9_9).
- 4 P. B. Patil, D. Sarkar and A. Sarkar, in *Relationship Between Microbes and the Environment for Sustainable Ecosystem Services*, ed. J. Samuel, A. Kumar and J. Singh, Elsevier, 2023, pp. 1–14, DOI: [10.1016/B978-0-323-89936-9.00006-0](https://doi.org/10.1016/B978-0-323-89936-9.00006-0).
- 5 J. Wang and Y. Yin, *Microb. Cell Fact.*, 2018, **17**, 22.
- 6 P. Pan and N. Bhattacharyya, *Curr. Microbiol.*, 2023, **80**, 252.
- 7 A. Antonucci, M. Reggente, C. Roullier, A. J. Gillen, N. Schuergers, V. Zubkovs, B. P. Lambert, M. Mouhib, E. Carata, L. Dini and A. A. Boghossian, *Nat. Nanotechnol.*, 2022, **17**, 1111–1119.
- 8 K. Obileke, H. Onyeaka, E. L. Meyer and N. Nwokolo, *Electrochem. Commun.*, 2021, **125**, 107003.
- 9 W. Haehnel and H. J. Hochheimer, *Bioelectrochem. Bioenerg.*, 1979, **6**, 563–574.
- 10 X. Wei, H. Lee and S. Choi, *Sens. Actuators, B*, 2016, **228**, 151–155.
- 11 K. L. Saar, P. Bombelli, D. J. Lea-Smith, T. Call, E.-M. Aro, T. Müller, C. J. Howe and T. P. J. Knowles, *Nat. Energy*, 2018, **3**, 75–81.
- 12 H. Zhu, H. Meng, W. Zhang, H. Gao, J. Zhou, Y. Zhang and Y. Li, *Nat. Commun.*, 2019, **10**, 4282.
- 13 J. Tschörtner, B. Lai and J. O. Krömer, *Front. Microbiol.*, 2019, 10.
- 14 L. T. Wey, P. Bombelli, X. Chen, J. M. Lawrence, C. M. Rabideau, S. J. L. Rowden, J. Z. Zhang and C. J. Howe, *ChemElectroChem*, 2019, **6**, 5375–5386.
- 15 M. Sawa, A. Fantuzzi, P. Bombelli, C. J. Howe, K. Hellgardt and P. J. Nixon, *Nat. Commun.*, 2017, **8**, 1327.
- 16 L. Reshma, A. Chaitanyakumar, A. L. G. N. Aditya, B. Ramaraj and K. Santhakumar, *Algal Res.*, 2017, **26**, 47–55.
- 17 M. Anam, H. I. Gomes, G. Rivers, R. L. Gomes and R. Wildman, *Sustainable Energy & Fuels*, 2021, **5**, 4209–4232.
- 18 L. Liu and S. Choi, *Lab Chip*, 2017, **17**, 3817–3825.
- 19 T. Wenzel, D. Härtter, P. Bombelli, C. J. Howe and U. Steiner, *Nat. Commun.*, 2018, **9**, 1299.
- 20 S. Kaushik, M. K. Sarma and P. Goswami, *J. Mater. Chem. A*, 2017, **5**, 7885–7895.
- 21 H. Lee and J. Hyun, *Carbohydr. Polym.*, 2023, **321**, 121299.
- 22 F. Bragheri, R. Martínez Vázquez and R. Osellame, in *Three-Dimensional Microfabrication Using Two-Photon Polymerization*, ed. T. Baldacchini, William Andrew Publishing, 2020, 2nd edn, pp. 493–526, DOI: [10.1016/B978-0-12-817827-0.00057-6](https://doi.org/10.1016/B978-0-12-817827-0.00057-6).
- 23 F. Eduati, R. Utharala, D. Madhavan, U. P. Neumann, T. Longerich, T. Cramer, J. Saez-Rodriguez and C. A. Merten, *Nat. Commun.*, 2018, **9**, 2434.
- 24 J. Zhai, S. Yi, Y. Jia, P.-I. Mak and R. P. Martins, *TrAC, Trends Anal. Chem.*, 2019, **117**, 231–241.
- 25 M. Yew, Y. Ren, K. S. Koh, C. Sun and C. Snape, *Global Challenges*, 2019, **3**, 1800060.
- 26 K. W. Oh, *Micromachines*, 2017, **8**, 343.
- 27 R. Gorkin, J. Park, J. Siegrist, M. Amasia, B. S. Lee, J.-M. Park, J. Kim, H. Kim, M. Madou and Y.-K. Cho, *Lab Chip*, 2010, **10**, 1758–1773.
- 28 B. Ozdalgic, M. Ustun, S. R. Dabbagh, B. Z. Haznedaroglu, A. Kiraz and S. Tasoglu, *Biotechnol. Bioeng.*, 2021, **118**, 1716–1734.
- 29 J. Y. H. Kim, H. S. Kwak, Y. J. Sung, H. I. Choi, M. E. Hong, H. S. Lim, J.-H. Lee, S. Y. Lee and S. J. Sim, *Sci. Rep.*, 2016, **6**, 21155.
- 30 H. S. Kim, T. P. Devarenne and A. Han, *Algal Res.*, 2018, **30**, 149–161.
- 31 P. Bodénès, H.-Y. Wang, T.-H. Lee, H.-Y. Chen and C.-Y. Wang, *Biotechnol. Biofuels*, 2019, **12**, 33.
- 32 Y.-J. Juang and J.-S. Chang, *Biotechnol. J.*, 2016, **11**, 327–335.
- 33 T. Heidorn, D. Camsund, H.-H. Huang, P. Lindberg, P. Oliveira, K. Stensjö and P. Lindblad, in *Methods in Enzymology*, ed. C. Voigt, Academic Press, 2011, vol. 497, pp. 539–579.
- 34 B. Berla, R. Saha, C. Immethun, C. Maranas, T. S. Moon and H. Pakrasi, *Front. Microbiol.*, 2013, 4.



- 35 A. C. Barros, A. L. Gonçalves and M. Simões, *J. Appl. Phycol.*, 2019, **31**, 375–387.
- 36 M. Sarma, S. Kaushik and P. Goswami, *Biomass Bioenergy*, 2016, **90**, 187–201.
- 37 P. Farrokh, M. Sheikhpour, A. Kasaeian, H. Asadi and R. Bavandi, *Biotechnol. Prog.*, 2019, **35**, e2835.
- 38 N. Nozzi, J. Oliver and S. Atsumi, *Front. Bioeng. Biotechnol.*, 2013, **1**.
- 39 M. Sawa, A. Fantuzzi, P. Bombelli, C. J. Howe, K. Hellgardt and P. J. Nixon, *Nat. Commun.*, 2017, **8**, 1327.
- 40 P. Imbimbo, L. D'Elia, I. Corrado, G. Alvarez-Rivera, A. Marzocchella, E. Ibáñez, C. Pezzella, F. Branco dos Santos and D. M. Monti, *Molecules*, 2023, **28**, 3144.
- 41 A. Sánchez-Bayo, V. Morales, R. Rodríguez, G. Vicente and L. F. Bautista, *Molecules*, 2020, **25**, 2834.
- 42 L. Grossmann, J. Hinrichs and J. Weiss, *Crit. Rev. Food Sci. Nutr.*, 2020, **60**, 2961–2989.
- 43 S. Rashad, A. S. El-Hassanin, S. S. M. Mostafa and G. A. El-Chaghaby, *Global J. Environ. Sci. Manage.*, 2019, **5**, 167–174.
- 44 T. Johnson, S. Katuwal, G. Anderson, L. Gu, R. Zhou and W. Gibbons, *Biotechnol. Prog.*, 2018, **34**.
- 45 S. M. F. Kabir, P. P. Sikdar, B. Haque, M. A. R. Bhuiyan, A. Ali and M. N. Islam, *Prog. Biomater.*, 2018, **7**, 153–174.
- 46 D. A. Gyles, L. D. Castro, J. O. C. Silva and R. M. Ribeiro-Costa, *Eur. Polym. J.*, 2017, **88**, 373–392.
- 47 D. A. Alfaro-Sayes, J. Amoah, S. Aikawa, M. Matsuda, T. Hasunuma, A. Kondo and C. Ogino, *Biochem. Eng. J.*, 2022, **188**, 108681.
- 48 J. Liu, R. Zhang, M. Ci, S. Sui and P. Zhu, *J. Eng. Fibers Fabr.*, 2019, **14**, 1558925019847553.
- 49 H. Seddiqi, E. Oliaei, H. Honarkar, J. Jin, L. C. Geonzon, R. G. Bacabac and J. Klein-Nulend, *Cellulose*, 2021, **28**, 1893–1931.
- 50 D. C. Wang, S. N. Lei, S. Zhong, X. Xiao and Q. H. Guo, *Polymers*, 2023, **15**.
- 51 R. Toczyłowska-Mamińska, K. Szymona, P. Król, K. Gliniewicz, K. Pielech-Przybylska, M. Kloch and B. E. Logan, *Energies*, 2018, **11**, 124.
- 52 I. Kazama, N. Hirose, Y. Aso, T. Tanaka and H. Ohara, *Biotechnol. Lett.*, 2023, **45**, 1467–1476.
- 53 Y. Takeuchi, W. Khawdas, Y. Aso and H. Ohara, *J. Biosci. Bioeng.*, 2017, **123**, 358–363.
- 54 Q. L. Loh and C. Choong, *Tissue Eng., Part B*, 2013, **19**, 485–502.
- 55 I. Mallick, P. Kirtania, M. Szabó, F. Bashir, I. Domonkos, P. B. Kós and I. Vass, *PLoS One*, 2020, **15**, e0236842.
- 56 S. S. Ramachandra, A. Abdal-hay, P. Han, R. S. B. Lee and S. Ivanovski, *Biomater. Adv.*, 2023, **145**, 213251.
- 57 W. Yang, J. Li, L. Zhang, X. Zhu and Q. Liao, *RSC Adv.*, 2017, **7**, 28469–28475.
- 58 N. N. Mohd Noor, N. I. Oktavetri and K. Kim, *Fuel*, 2024, **367**, 131438.
- 59 S. Cheng and B. E. Logan, *Bioresour. Technol.*, 2011, **102**, 4468–4473.
- 60 S. Choi, *Biotechnol. Adv.*, 2016, **34**, 321–330.
- 61 L. Liu and S. Choi, *SLAS Technol.*, 2020, **25**, 75–81.
- 62 K. Kuruvina Shetti and M. Packirisamy, *Microsyst. Nanoeng.*, 2022, **8**, 29.
- 63 P. Bombelli, T. Müller, T. W. Herling, C. J. Howe and T. P. J. Knowles, *Adv. Energy Mater.*, 2015, **5**, 1401299.
- 64 A. J. McCormick, P. Bombelli, A. M. Scott, A. J. Philips, A. G. Smith, A. C. Fisher and C. J. Howe, *Energy Environ. Sci.*, 2011, **4**, 4699–4709.
- 65 W. Yang, W. He, F. Zhang, M. A. Hickner and B. E. Logan, *Environ. Sci. Technol. Lett.*, 2014, **1**, 416–420.
- 66 B. Kim, I. S. Chang, R. M. Dinsdale and A. J. Guwy, *Electrochim. Acta*, 2021, **366**, 137388.
- 67 G. N. Hotos and T. I. Antoniadis, *Life*, 2022, **12**, 837.
- 68 J. Tschörtner, B. Lai and J. O. Krömer, *Front. Microbiol.*, 2019, **10**.
- 69 D. J. Lea-Smith and G. T. Hanke, *Cyanobacteria Biotechnology*, 2021, pp. 33–63, DOI: [10.1002/9783527824908.ch2](https://doi.org/10.1002/9783527824908.ch2).
- 70 G. Shimakawa, *J. Exp. Bot.*, 2023, **74**, 3476–3487.
- 71 A. ElMekawy, H. M. Hegab, X. Dominguez-Benetton and D. Pant, *Bioresour. Technol.*, 2013, **142**, 672–682.
- 72 İ. Bütün, S. Çelik, K. B. Dönmez, A. Yürüm, S. A. Gürsel and A. Koşar, *J. Energy Storage*, 2024, **90**, 111739.
- 73 İ. Bütün, G. Gharib, A. Yürüm, S. A. Gürsel and A. Koşar, *Int. J. Energy Res.*, 2022, **46**, 22653–22663.
- 74 A. Cereda, A. Hitchcock, M. D. Symes, L. Cronin, T. S. Bibby and A. K. Jones, *PLoS One*, 2014, **9**, e91484.
- 75 K. Hakki, T. Antal, A. U. Rehman, J. Kurkela, H. Wada, I. Vass, E. Tyystjärvi and T. Tyystjärvi, *Biochim. Biophys. Acta, Bioenerg.*, 2014, **1837**, 217–225.
- 76 L. Liu and S. Choi, *J. Power Sources*, 2021, **506**, 230251.
- 77 H.-Y. Wang, A. Bernarda, C.-Y. Huang, D.-J. Lee and J.-S. Chang, *Bioresour. Technol.*, 2011, **102**, 235–243.
- 78 J. Luo, W. Tian, H. Jin, J. Yang, J. Li, Y. Wang, W. Shen, Y. Ren and M. Zhou, *Curr. Opin. Electrochem.*, 2023, **37**, 101187.
- 79 A. West, in *Encyclopedia of Applied Electrochemistry*, ed. G. Kreysa, K.-I. Ota and R. F. Savinell, Springer, New York, NY, 2014, pp. 464–467, DOI: [10.1007/978-1-4419-6996-5\\_324](https://doi.org/10.1007/978-1-4419-6996-5_324).
- 80 M. Mehdizadeh Allaf and H. Peerhossaini, *Microorganisms*, 2022, **10**, 696.
- 81 Matthew P. Johnson, *Essays Biochem.*, 2016, **60**, 255–273.
- 82 P. Bombelli, M. Zarrouati, R. J. Thorne, K. Schneider, S. J. L. Rowden, A. Ali, K. Yunus, P. J. Cameron, A. C. Fisher, D. Ian Wilson, C. J. Howe and A. J. McCormick, *Phys. Chem. Chem. Phys.*, 2012, **14**, 12221–12229.
- 83 B. E. Logan, *Microbial fuel cells*, John Wiley & Sons, 2008.
- 84 H. Nasution, E. B. Yahya, H. P. S. Abdul Khalil, M. A. Shaah, A. B. Suriani, A. Mohamed, T. Alfatah and C. K. Abdullah, *Polymers*, 2022, **14**, 326.
- 85 T.-Y. Yu, Y.-H. Tseng, M.-C. Wu, C.-S. Tsao and W.-F. Su, *Cham*, 2022.
- 86 A. K. Rana, V. K. Gupta, P. Hart and V. K. Thakur, *Environ. Res.*, 2024, **243**, 117889.
- 87 I. N. Besiri, T. B. Goudoulas and N. Germann, *Phys. Fluids*, 2022, **34**.
- 88 M. B. Łabowska, M. Skrodzka, H. Sicińska, I. Michalak and J. Detyna, *Gels*, 2023, **9**, 63.





- 89 V. Rissanen, S. Vajravel, S. Kosourov, S. Arola, E. Kontturi, Y. Allahverdiyeva and T. Tammelin, *Green Chem.*, 2021, **23**, 3715–3724.
- 90 E. Touloupakis, G. Rontogiannis, A. M. Silva Benavides, B. Cicchi, D. F. Ghanotakis and G. Torzillo, *Int. J. Hydrogen Energy*, 2016, **41**, 15181–15186.
- 91 M. Grzesiuk, B. Pietrzak, A. Wacker and J. Pijanowska, *Front. Plant Sci.*, 2022, 13.
- 92 N. Wang, L. Bian, X. Ma, Y. Meng, C. S. Chen, M. U. Rahman, T. Zhang, Z. Li, P. Wang and Y. Chen, *J. Biol. Chem.*, 2019, **294**, 16309–16319.

